SCIPEDIA

Free Vibration Analysis of Non-Uniform Timoshenko Beams Using Haar Wavelets

Tarık Baran*

Department of Civil Engineering, Osmaniye Korkut Ata University, Osmaniye, 80000, Turkey

INFORMATION

Keywords:
Axially functionally graded
tapered Timoshenko beams
free vibrations
Haar wavelet method
natural frequencies
numerical analysis

DOI: 10.23967/j.rimni.2024.10.58106

SCIPEDIA Revista Internacional de Métodos Numéricos para Cálculo y Diseño en Ingeniería

RIMNI Revista Internacional Métodos numéricos para cálculo y diseño en ingeniería

Free Vibration Analysis of Non-Uniform Timoshenko Beams Using Haar Wavelets

Tarık Baran*

Department of Civil Engineering, Osmaniye Korkut Ata University, Osmaniye, 80000, Turkey

ABSTRACT

In this paper, we present a method using Haar wavelets for solving axially functionally graded (FG) Timoshenko beam equations with non-uniform cross-sections. We compare two different approaches to the solution. The first approach involves approximating the resulting function (i.e., rotation) of the differential equation with a polynomial function using Haar wavelets, which is a classical application in the Haar wavelet method. The second method employs an auxiliary function that uses Haar wavelets, but the rotation or deflection do not directly equal the sought function. The rotation and deflection are derived from this auxiliary function. In both methods, the coupled governing equations are transformed into a single governing equation. Using the Haar wavelet method, this single differential equation transforms into a system of linear algebraic equations. For different boundary conditions, the roots of the characteristic polynomial equation obtained from the system of linear algebraic equations are solved to determine the lowest to highest-order natural frequencies. Our results show that the use of auxiliary function is faster and more consistent with the results available in the literature. We presented several natural frequency predictions of Timoshenko beams with different taper ratios and support conditions that have not been detailed in the literature before.

OPEN ACCESS

Received: 04/09/2024

Accepted: 07/11/2024

DOI
10.23967/j.rimni.2024.10.58106

Keywords:
Axially functionally graded tapered Timoshenko beams
free vibrations
Haar wavelet method
natural frequencies
numerical analysis

1 Introduction

Timoshenko beam theory, which has been called [1,2] Timoshenko beam theory or Timoshenko–Ehrenfest beam theory [2] since it first appeared in 1922, is the first major advance in beam theory after the Euler–Bernoulli beam theory. Unlike Euler–Bernoulli beam theory, rotation of a cross-section along with transverse deflection is considered in the governing equations. In this case, two governing coupled second-order differential equations are obtained. The governing equations of a straight-axis beam depend on a single spatial coordinate along the beam length, and time. The rotation of a cross-section and the transverse deflection are obtained from the solution of the equations.

It is a well-known fact that the Euler–Bernoulli beam theory provides accurate results in the analysis of long and slender beams but can produce erroneous results for short and thick beams

*Correspondence: Tarık Baran (tarikbaran@osmaniye.edu.tr).

[3]. Therefore, the Timoshenko beam theory is quite useful for analysing short and thick beam-like structures, ranging from large [4] to macro [5] and nano scale [6]. Because of technological and aesthetic needs, beam-like structures with non-homogeneous materials and non-uniform cross-section shapes are required to optimize the weight and strength of the structure, both in line with electronics and architecture. Modal analysis, which is often necessary for determining the dynamic behaviour of beam-type structures, can be performed using the Timoshenko beam model due to its success in predicting accurate frequencies across a range from low to higher modes of vibration. However, the governing equations of Timoshenko beam theory are quite complex and difficult to solve when dealing with non-homogeneous materials and non-uniform sections. Consequently, researchers have been working for many years on developing faster solution methods that yield accurate results [3,7]. Most researchers have examined material gradation along the beam thickness direction when dealing with non-homogeneous materials in Timoshenko beam analyses [8–10]. However, studies on beams with material gradation and non-uniform cross-sections along the beam axis are relatively fewer. The milestone works on the vibration of Timoshenko beams, which address the gradation of beam material and section properties along the axis, are chronologically as follows: The modal analysis of Timoshenko beams was conducted by Huang [11]. These analyses are for beams with uniform cross-sections. While the solutions to the equations are relatively straightforward for beams with uniform cross-sections, they become more complex when considering non-uniform cross-sections. When considering the non-uniform cross-sections, varying cross-sectional properties along the length make the solution more complicated. If the change in material properties along the length is also considered, the solution becomes even more complex. To overcome the difficulty in solving the non-uniform Timoshenko beam, the finite element method was mainly utilized. Thomas et al. [12] developed finite element formulations for Timoshenko beams, providing a comprehensive approach to handle both bending and shear deformations. Heppler et al. [13] introduced a finite element method using trigonometric basis functions to improve the accuracy of Timoshenko beam analysis, showing enhanced accuracy and convergence rates, particularly under complex loading and boundary conditions. Ju et al. [14] investigated the free vibration characteristics of stepped beams using analytical methods, offering detailed insights into the effects of step changes in cross-sectional properties on the natural frequencies. Rossi et al. [15] analysed the transverse vibrations of a Timoshenko beam with non-uniform thickness, clamped at one end and carrying a concentrated mass at the other, providing accurate analytical solutions and highlighting the significant influence of these factors on vibration behaviour. Loula et al. [16] developed Petrov-Galerkin formulations for Timoshenko beam problems, enhancing numerical stability and accuracy. Grosh et al. [17] introduced Galerkin generalized least squares methods for solving Timoshenko beam equations. Their method demonstrates superior stability and accuracy in numerical analysis. These results make their methods valuable for complex structural simulations.

Using different solution methods, researchers have continued to address the solution of the Timoshenko beams considering material non-homogeneity along the length, added mass, and springs. Lee et al. [18] presented exact vibration solutions for nonuniform Timoshenko beams with mass attachments, utilizing analytical methods to explore the beam's dynamic characteristics. Tong et al. [19] investigated the vibration analysis of Timoshenko beams with non-homogeneity and varying cross-sections, employing analytical techniques to understand the impact of cross-sectional variations on vibration modes. Leung et al. [20] have explored the non-uniform Timoshenko column vibration using the dynamic stiffness method. They have presented a power series approach to the dynamic stiffness matrix of the Timoshenko beams. Shahba et al. [3] conducted free vibration analyses of non-homogeneous, variable cross-section Timoshenko beams using the finite element approach. Their

finite element formulation uses exact shape functions. They reported that they have adopted the shape functions from Reddy [21]. Huang et al. [7] investigated the free vibration behaviour of axially functionally graded Timoshenko beams with non-uniform cross-sections, highlighting the influence of material gradients on natural frequencies. They have presented a polynomial auxiliary function to obtain a fourth-order differential governing equation from coupled two second-order differential equations. Yuan et al. [22] derived exact solutions for the free vibrations of axially inhomogeneous Timoshenko beams with variable cross sections, emphasizing the analytical approach to predict vibration modes accurately. Their methods are suitable for solving cases where material and cross-sectional area variations are exponential and power series. Wang et al. [23] analysed the free vibration characteristics of metal foam core sandwich beams on elastic foundations, focusing on structural damping and foundation effects.

In recent years researchers have continued the FG Timoshenko beams for different cases employing various solution methods. Chen [24] has studied the vibration analysis of axially functionally graded Timoshenko beams with non-uniform cross-sections, providing insights into the effects of material grading on beam dynamics. Zhang et al. [25] have investigated the buckling and free vibration sandwich Timoshenko beams resting on elastic foundation. They have considered both beam and the foundation nonlocal. The generalized differential quadrative method (GDQM) is utilized to obtain frequencies. Their study revealed that size-dependent characteristics should be given greater consideration in structural problems. Zhang et al. [26] have presented a unified local-nonlocal integral formulation for analysing the dynamic stability of functionally graded (FG) porous viscoelastic Timoshenko beams resting on a nonlocal Winkler-Pasternak foundation, and the model incorporates both strain- and stress-driven local-nonlocal elasticity theories. Numerical examples demonstrate how foundation forces and nonlocal effects influence beam stability. Sinha [27] has presented a free vibration analysis method for Timoshenko beams considering arbitrary non-uniform material with discontinuities and constraints. His algorithm gives exact solutions when the continuous beam segment between discontinuities is uniform. Burlayenko et al. [28] have presented a comparison of one-dimensional and three-dimensional models to simulate the free vibrations of axially functionally graded material (AFGM) beams with non-uniform cross-sections. They employed commercial finite element method software and developed user-defined material model subroutines (UMAT). They reported that as the geometric complexity and material inhomogeneity of the AFGM beams increase, the differences between the one-dimensional and three-dimensional models become more pronounced at higher-order frequencies. Subsequently, Burlayenko et al. [29] focused on the free vibration analysis of axially functionally graded material (AFGM) beams with curvilinear tapered cross-sections. Their study provides insights into how factors like material gradation, beam shape, and slenderness ratio affect the natural frequencies of AFGM beams. In another study, Burlayenko et al. [30] explored the modal characteristics of functionally graded porous Timoshenko beams with variable cross-sections. They presented a parametric study on the effects of porosity and taper ratios on the vibrational behaviour of FG Timoshenko beams. Deneme et al. [31] investigated the dynamic behaviour of AFGM variable cross-section Timoshenko beams employing the Complementary Functions Method. They validated their method using commercial finite element software and literature examples and stated that their method is efficient in solving this type of problem.

Experimental work is essential for validating theoretical and numerical methods. However, only a limited number of experimental studies have been conducted on the vibration of Timoshenko beams [32–36], and none have independently considered material nonhomogeneity or cross-sectional variations—or both. One of the earliest examples of these works was published by Kaneko [32] focusing on the relationship between the shear coefficient and flexural vibrations. In subsequent

years, Mendez-Sanchez et al. [33] examined the consistency between experimental frequencies and mode shapes with theoretical predictions for different Timoshenko shear coefficients. Two related studies by Díaz-De-Anda et al. [34] and Monsivais et al. [35] have made significant contributions to the experimental investigation of Timoshenko beam vibrations. Both studies compare experimental results with theoretical and numerical findings. A recent example of experimental work is provided by Brøns et al. [36], who used a laser Doppler vibrometer to measure frequencies and mode shapes of bending vibrations above the critical frequency predicted by Timoshenko theory. The authors compared experimental results with theoretical and numerical predictions, noting a maximum deviation of 5% for frequencies above the critical threshold. For frequencies below the critical threshold, however, they reported greater deviations between experimental, theoretical, and numerical results.

This work aims to find the free vibration frequencies of axially nonhomogeneous, variable-sectioned Timoshenko beams for different boundary conditions, using the Haar Wavelet method [37], which is very successful in high-order and complex differential equation solver. To the best of the author's knowledge, the Haar Wavelet method, which has been successfully applied to the solution of Euler-Bernoulli beam equations [37,38], has only been used by Lepik et al. [37] in the free vibration analysis of Timoshenko beams. However, the results presented in the relevant source are limited and insufficient, and no other sources are available. This limitation may be due to the method's performance, which does not yield good results in some support conditions and may require large calculation times. Another study by Mehrparvar et al. [39] serves as an example of the solution of Timoshenko beams using the Haar wavelet method. They employed the higher-order Haar wavelet method to solve the beam equations; however, they considered only variable cross-sections, not material gradation.

In this study, instead of directly assuming the function obtained after the solution as the beam section's rotation, which is traditionally used in the Haar Wavelet method, an auxiliary function approach adapted from Huang et al. [7] was employed. This approach yields consistent results with the literature, reduces calculation times, and produces accurate results at lower resolutions. Structure of the paper is as follows: a brief introduction to the Haar Wavelet method and its application to the Timoshenko beam theory equations using both classical and auxiliary functions; verifications of the proposed method; and finally, several frequency results for different boundary conditions of tapered, non-homogeneous beams, which are not detailed in the literature.

2 Method

2.1 Brief Introduction to the Solution of Differential Equations Using Haar Wavelet Method

In this section, we present only the method for equal grid spacing for the sake of simplicity and brevity. Please refer to Lepik et al. [37] for formulations of Haar matrices required for unequal grid spacing (non-uniform Haar wavelets).

The method mentioned here is the n-th order ordinary differential equation (ODE) solution method proposed by Chen et al. [40] for first-order ODE's and described in detail by Lepik et al. [37] for higher-order ODE's. Although the method is an initial value problem solution method, the solution is obtained by transforming boundary value problems into initial value problems with the Haar wavelets. Following Lepik et al. [37], the n-th order linear differential equation with initial conditions may be given as:

$$\sum_{\nu=0}^{n} A_{\nu}(x)\, y^{(\nu)}(x) = f(x),\ x \in [A,\ B] \tag{1}$$

$$y^{(v)}(A) = y_0^{(v)},\ v = 0,\ 1, \ldots,\ n-1. \tag{2}$$

where x is an independent variable with boundaries A, B, $y^{(v)}(x)$ is x the dependent function and derivative of functions, $A_v(x)$, and $f(x)$ are prescribed functions, v is the order of the derivative, $y_0^{(v)}$ is the initial condition of the v-th order derivative, and n is the order of the ODE.

The highest-order derivative is taken equal to the Haar wavelet series,

$$y^{(n)}(x) = \sum_{i=1}^{2M} a_i h_i(x) \tag{3}$$

where i is an index variable for the wavelet number, $2M$ is the number of grid points ($M = 2^J$ where J is the maximum level of resolution), a_i are wavelet coefficients, and $h_i(x)$ is the i-th (where $i > 2$) Haar wavelet and may be given with equal grid spacing

$$h_i(x) = \begin{cases} 1 \text{ for} & x \in [\xi_1(i),\ \xi_2(i)), \\ -1 \text{ for} & x \in [\xi_2(i),\ \xi_3(i)), \\ 0 & \text{elsewhere.} \end{cases} \tag{4}$$

where

$$\begin{aligned} \xi_1(i) &= A + 2k\mu\Delta x, \qquad \xi_2(i) = A + (2k+1)\mu\Delta x, \\ \xi_3(i) &= A + 2(k+1)\mu\Delta x, \qquad \mu = \tfrac{M}{m} \end{aligned} \tag{5}$$

appearing terms in Eq. (5) are $m = 2^j$ by introducing $j = 0,\ 1, \ldots,\ J$ and $k = 0,\ 1, \ldots,\ m-1$. The wavelet number i may be given with $i = m + k + 1$. The grid interval step may be defined as $\Delta x = (B - A)/(2M)$.

For the case where $i = 1$, $h_i(x)$ may be given with $h_i(x) = 1$. When $i = 2$, $\xi_1(2)$, $\xi_2(2)$ and $\xi_3(2)$ should be calculated as $\xi_1(2) = A$, $\xi_2(2) = 0.5(2A + B)$ and $\xi_3(2) = B$ respectively for substitution in Eq. (4).

$n - v$ times integration gives the solution in the following form:

$$y^{(v)}(x) = \sum_{i=1}^{2M} a_i p_{n-v,i}(x) + Z_v(x), \tag{6}$$

where

$$Z_v(x) = \sum_{\sigma=0}^{n-v-1} \frac{1}{\sigma!}(x - A)^{\sigma} y^{(v+\sigma)}(A), \tag{7}$$

where $p_{n-v,i}(x)$ is the $(n-v)$-th integral of the Haar wavelet, σ is the index variable and A is the initial point of x. Changing $(n - v)$ with α, the integral of the Haar wavelets may be given for $i > 1$

$$p_{\alpha,i}(x) = \begin{cases} 0 & \text{for } x < \xi_1(i), \\ \frac{1}{\alpha!}[x - \xi_1(i)]^{\alpha} & \text{for } x \in [\xi_1(i),\ \xi_2(i)], \\ \frac{1}{\alpha!}[(x - \xi_1(i))^{\alpha} - 2(x - \xi_2(i))^{\alpha}] & \text{for } x \in [\xi_2(i),\ \xi_3(i)], \\ \frac{1}{\alpha!}[(x - \xi_1(i))^{\alpha} - 2(x - \xi_2(i))^{\alpha} + (x - \xi_3(i))^{\alpha}] & \text{for } x > \xi_3(i). \end{cases} \tag{8}$$

When $i = 1$ one should consider $\xi_1(1) = A$, $\xi_2(1) = \xi_3(1) = B$. Then the first wavelet integral may be given

$$p_{\alpha,1}(x) = \frac{1}{\alpha!}(x - A)^{\alpha}. \tag{9}$$

For the numerical solution, Haar wavelet discretization is required. A definition may be made to calculate grid points at equal intervals

$$\widetilde{x}_l = A + l\Delta x,\ l = 0,\ 1, \ldots,\ 2M. \tag{10}$$

where l is the grid index and $\widetilde{x}_l$ are the grid points. Then using the collocation method, collocation points may be calculated with

$$x_l = 0.5\left(\tilde{x}_{l-1} + \tilde{x}_l\right),\ l = 1, \ldots,\ 2M. \tag{11}$$

By replacing x and $\tilde{x}$ with x_l in the above equations and writing Eq. (1) in discrete form, one may obtain the linear system of equations from ODE. Putting the linear system of equations in matrix form is advantageous. Thus, we can introduce the $2M \times 2M$ Haar operational matrices as H, P_1, $P_2, \ldots, P_\nu$ with their elements in the form of $H(i,l) = h_i(x_l)$, $P_\nu(i,\ l) = p_{\nu,i}(x_l)$, $\nu = 1,\ 2, \ldots$ After successfully solving the linear system of equations, unknown wavelet coefficients (a_i) can be easily determined. Then, using Eqs. (6) and (7), one may reorganize the sought function $y(x)$.

2.2 Free Vibration Evaluation of Timoshenko Beams Using Haar Wavelet Method: Conventional Approach (HWM-C)

For the sake of brevity, we do not again derive the governing equations of the FG Timoshenko beams with variable cross-sections along the length. We adopted the equations from Shahba et al. [3]. Please refer to Shahba et al. [3] and Huang et al. [7] for the derivation of the governing equations.

The second-order coupled differential equations that govern the free vibration of a Timoshenko beam with a length of L, variable cross-sections and material properties along its length are as follows [3]:

$$\begin{gathered}\frac{d}{dx}\left(E(\tilde{x})\, I(\tilde{x})\frac{d\theta(\tilde{x})}{d\tilde{x}}\right) + kG(\tilde{x})\, A(\tilde{x})\left(\frac{dw(\tilde{x})}{d\tilde{x}} - \theta(\tilde{x})\right) + \rho(\tilde{x})\, I(\tilde{x})\,\omega^2\theta(\tilde{x}) = 0, \\ \frac{d}{d\tilde{x}}\left(kG(\tilde{x})\, A(\tilde{x})\left(\frac{dw(\tilde{x})}{d\tilde{x}} - \theta(\tilde{x})\right)\right) + \rho(\tilde{x})\, A(\tilde{x})\,\omega^2 w(\tilde{x}) = 0.\end{gathered} \tag{12}$$

where $\tilde{x}$ is the lengthwise axis variable, $E(\tilde{x})$ is the modulus of elasticity, $G(\tilde{x})$ is the shear modulus or rigidity and is defined by $G(\tilde{x}) = \dfrac{E(\tilde{x})}{2(1+\nu)}$ (where ν is the Poisson's ratio), $I(\tilde{x})$ is the moment of inertia, k is the shear correction factor, $A(\tilde{x})$ is the cross-sectional area, $\rho(\tilde{x})$ is the mass density, and ω is the circular frequency. $w(\tilde{x})$ and $\theta(\tilde{x})$ are the transverse displacement and the bending rotation, respectively which are the sought functions. The terms $E(\tilde{x})$ and $\rho(\tilde{x})$ in Eq. (12) govern the material gradation along the length, whereas the effect of the variation in the cross-section is considered with $A(\tilde{x})$ and $I(\tilde{x})$.

Expressing the equations dimensionless based on length provides ease of formulation. It should be noted that since the equally spaced Haar wavelets are defined between 0 and 1, dimensionless equations are essential. Thus, the beam length is equal to 1. Following Lepik et al. [37], the required steps may

be given as follows:

$$\begin{aligned} &E\left(\tilde{x}\right)=E_0E_1\left(\tilde{x}\right),\ \rho\left(\tilde{x}\right)=\rho_0\rho_1\left(\tilde{x}\right),\\ &A\left(\tilde{x}\right)=A_0A_1\left(\tilde{x}\right),\ I\left(\tilde{x}\right)=I_0I_1\left(\tilde{x}\right), \end{aligned} \tag{13}$$

where $E_0=E\left(0\right)$, $\rho_0=\rho\left(0\right)$, $A_0=A\left(0\right)$, and $I_0=I\left(0\right)$.

After introducing the dimensionless parameters,

$$x=\frac{\tilde{x}}{L},\ \varpi^2=\omega^2\frac{\rho_0A_0L^4}{E_0I_0},\ s^2=\frac{2r^2\left(1+\nu\right)}{k},\ r^2=\frac{I_0}{A_0L^2}, \tag{14}$$

we may reorganise the governing equations of vibration for the Timoshenko beam with unit length as

$$\begin{aligned} &s^2\left[E_1\left(x\right)I_1\left(x\right)\theta\left(x\right)'\right]'+E_1\left(x\right)A_1\left(x\right)\left[w'\left(x\right)-\theta\left(x\right)\right]+r^2s^2\varpi^2\rho_1\left(x\right)I_1\left(x\right)\theta\left(x\right)=0,\\ &\left[E_1\left(x\right)A_1\left(x\right)\left(w'(x)-\theta(x)\right)\right]'+s^2\varpi^2\rho_1\left(x\right)A_1\left(x\right)w\left(x\right)=0. \end{aligned} \tag{15}$$

where primes denote differentiation with respect to x. To apply the Haar wavelet method, two coupled equations need to be reduced to a single equation. First, the term $\left(E_1\left(x\right)A_1\left(x\right)\left[w'\left(x\right)-\theta\left(x\right)\right]\right)$ should be evaluated from the first equation and then substituted into the second equation. From the resulting equation, the function of transverse displacement $\left(w\left(x\right)\right)$ may be given as

$$w\left(x\right)=F_5\left(x\right)\theta'''\left(x\right)+F_6\left(x\right)\theta''\left(x\right)+F_7\left(x\right)\theta'\left(x\right)+F_8\left(x\right)\theta\left(x\right) \tag{16}$$

where

$$\begin{aligned} &F_5\left(x\right)=\frac{E_1\left(x\right)I_1\left(x\right)}{\varpi^2\rho_1\left(x\right)A_1\left(x\right)},\ F_6\left(x\right)=\frac{2\left(E_1\left(x\right)I_1\left(x\right)\right)'}{\varpi^2\rho_1\left(x\right)A_1\left(x\right)},\\ &F_7\left(x\right)=\frac{r^2\varpi^2\rho_1\left(x\right)I_1\left(x\right)+\left(E_1\left(x\right)I_1\left(x\right)\right)''}{\varpi^2\rho_1\left(x\right)A_1\left(x\right)},F_8\left(x\right)=\frac{r^2\left(\rho_1\left(x\right)I_1\left(x\right)\right)'}{\rho_1\left(x\right)A_1\left(x\right)}. \end{aligned} \tag{17}$$

After evaluating $w'\left(x\right)$ using Eq. (16) and substituting it into the equation at the first line of Eq. (15), the resulting simplified equation that needs to be solved may be given as

$$F_4\left(x\right)\theta^{IV}\left(x\right)+F_3\left(x\right)\theta'''\left(x\right)+F_2\left(x\right)\theta''\left(x\right)+F_1\left(x\right)\theta'\left(x\right)+F_0\left(x\right)\theta\left(x\right)=0, \tag{18}$$

where

$$\begin{aligned} &F_4\left(x\right)=F_5\left(x\right),\\ &F_3\left(x\right)=F_5'\left(x\right)+F_6\left(x\right),\\ &F_2\left(x\right)=F_6'\left(x\right)+F_7\left(x\right)+\frac{s^2I_1\left(x\right)}{A_1\left(x\right)},\\ &F_1\left(x\right)=F_7'\left(x\right)+F_8\left(x\right)+\frac{s^2\left(E_1\left(x\right)I_1\left(x\right)\right)'}{E_1\left(x\right)A_1\left(x\right)},\\ &F_0\left(x\right)=F_8'\left(x\right)-1+\frac{r^2s^2\varpi^2\rho_1\left(x\right)I_1\left(x\right)}{E_1\left(x\right)A_1\left(x\right)}. \end{aligned} \tag{19}$$

Now, the Haar wavelet method may be applied. Using Eqs. (3), (6) and (7) and replacing $y(x)$ with $\theta(x)$ the following relations may be obtained

$$\begin{aligned}
\theta^{IV}(x) &= \sum_{i=1}^{2M} a_i h_i(x), \\
\theta'''(x) &= \sum_{i=1}^{2M} a_i p_{1,i}(x) + \theta_0''', \\
\theta''(x) &= \sum_{i=1}^{2M} a_i p_{2,i}(x) + \theta_0''' x + \theta_0'', \\
\theta'(x) &= \sum_{i=1}^{2M} a_i p_{3,i}(x) + \frac{1}{2}\theta_0''' x^2 + \theta_0'' x + \theta_0', \\
\theta(x) &= \sum_{i=1}^{2M} a_i p_{4,i}(x) + \frac{1}{6}\theta_0''' x^3 + \frac{1}{2}\theta_0'' x^2 + \theta_0' x + \theta_0.
\end{aligned} \tag{20}$$

where $\theta_0 = \theta(0)$, $\theta_0' = \theta'(0)$, $\theta_0'' = \theta''(0)$, $\theta_0''' = \theta'''(0)$. Unknown quantities can be calculated from boundary conditions at $x = 0$ and $x = 1$ using Eqs. (16) and (20). After the unknown quantities are evaluated, the terms in Eq. (20) are substituted into Eq. (18) and x is replaced with x_l. Thus, the discrete governing equation may then be obtained at $2M$ discrete points as

$$\begin{aligned}
&F_4(x_l)\sum_{i=1}^{2M} a_i h_i(x_l) + F_3(x_l)\left(\sum_{i=1}^{2M} a_i p_{1,i}(x_l) + \theta_0'''\right) + F_2(x_l)\left(\sum_{i=1}^{2M} a_i p_{2,i}(x_l) + \theta_0''' x_l + \theta_0''\right) \\
&\quad + F_1(x_l)\left(\sum_{i=1}^{2M} a_i p_{3,i}(x_l) + \frac{1}{2}\theta_0''' {x_l}^2 + \theta_0'' x_l + \theta_0'\right) \\
&\quad + F_0(x_l)\left(\sum_{i=1}^{2M} a_i p_{4,i}(x_l) + \frac{1}{6}\theta_0''' {x_l}^3 + \frac{1}{2}\theta_0'' {x_l}^2 + \theta_0' x_l + \theta_0\right) = 0.
\end{aligned} \tag{21}$$

The Jacobian of Eq. (21) with respect to a_i vanishes the a_i terms and constants and derives the $2M \times 2M$ linear, homogeneous governing square matrix of the vibration. In this situation, only unknown is the square of the cyclic frequency parameter (ϖ^2) is unknown. The matrix equation of vibration is formed as follows:

$$\mathbf{K} - \varpi^2 \mathbf{M} = \mathbf{0}. \tag{22}$$

where $\mathbf{K}$ is the stiffness matrix, which includes flexural, shear, and geometric stiffness terms, and $\mathbf{M}$ is the mass matrix. For a nontrivial solution, the determinant of the system in Eq. (22) must be zero. The square roots of the roots of the characteristic equation are the circular frequencies that are sought. The mode shapes may be determined for every circular frequency employing the discrete form of Eq. (16).

Boundary Conditions for HWM-C

To evaluate the boundary conditions, some kinematic relationships should be introduced. The moment and shear force relationships with the transverse beam displacement and cross-section rotation may be given as

$$Q = kG(x)A(x)(w'(x) - \theta(x)), \tag{23}$$

$$M = -E(x)I(x)\theta'(x). \tag{24}$$

where M is the momen and Q is the shear force. This study examines the boundary conditions for five different support cases. These cases are: *i*) clamped-free (C-F), *ii*) clamped-clamped (C-C), *iii*) clamped-pinned (C-P), *iv*) pinned-pinned (P-P), and *v*) free-free (F-F). The initial unknown quantities

i.e., θ_0, θ_0', θ_0'', and θ_0''' at $x = 0$, which are necessary for solving Eq. (21), are evaluated from Eqs. (16) and (20). The first derivative of Eq. (16) should be determined owing to the shear force relation (see Eq. (23)) for the C-F and F-F cases. Boundary conditions yield a system of linear algebraic equations with three equations for tree unknowns. The remaining unknown (usually θ_0 or owing to the moment relation θ_0' (see Eq. (24))) is already known at $x = 0$. Table 1 summarizes the boundary conditions for all the cases.

Table 1: Boundary conditions for supporting cases

Case	x = 0	x = 1
C-F	$\theta(0) = 0,\ w(0) = 0$	$M(1) = 0,\ Q(1) = 0$
C-C	$\theta(0) = 0,\ w(0) = 0$	$\theta(1) = 0,\ w(1) = 0$
C-P	$\theta(0) = 0,\ w(0) = 0$	$M(1) = 0,\ w(1) = 0$
P-P	$M(0) = 0,\ w(0) = 0$	$M(1) = 0,\ w(1) = 0$
F-F	$M(0) = 0,\ Q(0) = 0$	$M(1) = 0,\ Q(1) = 0$

2.3 Free Vibration Evaluation of Timoshenko Beams Using Haar Wavelet Method: Auxiliary Function Approach (HWM-A)

We introduce the Haar wavelet method with an auxiliary function application. To the best of the author's knowledge, this approach has not been used in the Haar wavelet applications. The method is based on the work of Huang et al. [7]. In this approach, the sought function is an auxiliary function that is not directly equal to the cross-section rotation. The rotation, transverse displacement, moment and shear force are evaluated with newly defined functions that are derived from the auxiliary function. In this work, we choose a Haar wavelet function as an auxiliary function. We may start with the derived governing equation of the vibration by Huang et al. [7]

$$\sum_{i=1}^{4} A_i(x)\frac{\partial^i \Gamma(x,t)}{\partial x^i} - \left(\sum_{i=0}^{2} B_i(x)\frac{\partial^i \Gamma(x,t)}{\partial x^i}\right)\frac{\partial^2 \Gamma(x,t)}{\partial t^2} + C(x)\frac{\partial^4 \Gamma(x,t)}{\partial t^4} = 0, \tag{25}$$

where i is the index variable, t is the time variable, and Γ is the auxiliary function that is sought for. $A_i(x)$, $B_i(x)$, and $C(x)$ are functions that contain the stiffness, and mass terms. And they may be given with

$$A_1(x) = \left[E(x)I(x)\left(\frac{1}{\rho(x)A(x)}\right)''\right]',$$

$$A_2(x) = \left[2E(x)I(x)\left(\frac{1}{\rho(x)A(x)}\right)'\right]' + E(x)I(x)\left(\frac{1}{\rho(x)A(x)}\right)'',$$

$$A_3(x) = 2E(x)I(x)\left(\frac{1}{\rho(x)A(x)}\right)' + \left(\frac{E(x)I(x)}{\rho(x)}\right)',$$

$$A_4(x) = \frac{E(x)I(x)}{\rho(x)A(x)},$$

$$B_0(x) = \left[E(x)I(x)\left(\frac{1}{kG(x)A(x)}\right)'\right]' - 1,$$

$$B_1(x) = \left[\frac{E(x)I(x)}{kG(x)A(x)}\right]' + E(x)I(x)\left(\frac{1}{kG(x)A(x)}\right)' + \rho(x)I(x)\left(\frac{1}{\rho(x)A(x)}\right)',$$

$$B_2(x) = \frac{E(x)I(x)}{kG(x)A(x)} + \frac{\rho(x)I(x)}{\rho(x)A(x)}, \quad C(x) = \frac{\rho(x)I(x)}{kG(x)A(x)}. \tag{26}$$

By choosing the auxiliary function as in the form

$$\Gamma(x,\ t) = f(x)\, e^{i\varpi t}, \tag{27}$$

the governing equation of the vibration of the FG material, a variable cross-sectioned Timoshenko beam may be given with

$$\sum_{i=1}^{4} A_i(x) \frac{d^i f(x)}{dx^i} + \varpi^2 \left(\sum_{i=0}^{2} B_i(x) \frac{d^i f(x)}{dx^i} \right) + \varpi^2 C(x) f(x) = 0. \tag{28}$$

The expanded form of Eq. (28) is identical to that of Eq. (18), except for minor changes in the coefficient functions of the derivative terms.

By changing θ's with f in Eq. (21) and defining new coefficients for derivative terms, the governing equation of vibration using the auxiliary function may be given as

$$\begin{aligned}
&\Theta_4(x_l) \sum_{i=1}^{2M} a_i h_i(x_l) + \Theta_3(x_l) \left(\sum_{i=1}^{2M} a_i p_{1,i}(x_l) + f_0''' \right) + \Theta_2(x_l) \left(\sum_{i=1}^{2M} a_i p_{2,i}(x_l) + f_0''' x_l + f_0'' \right) \\
&\qquad + \Theta_1(x_l) \left(\sum_{i=1}^{2M} a_i p_{3,i}(x_l) + \frac{1}{2} f_0''' x_l^2 + f_0'' x_l + f_0' \right) \\
&\qquad + \Theta_0(x_l) \left(\sum_{i=1}^{2M} a_i p_{4,i}(x_l) + \frac{1}{6} f_0''' x_l^3 + \frac{1}{2} f_0'' x_l^2 + f_0' x_l + f_0 \right) = 0.
\end{aligned} \tag{29}$$

Knowing $G(x) = \dfrac{E(x)}{2(1+v)}$, and using Eq. (13) the coefficients may be defined as dimensionless. Thus, appearing Θ terms in Eq. (29) may be given

$$\begin{aligned}
\Theta_0(x) &= \varpi^2 \left(\left(E_1(x) I_1(x) \left(\frac{1}{G_1(x)} \right)' \right)' - 1 + \varpi^2 \left(\frac{\rho_1(x) I_1(x)}{G_1(x)} \right) \right), \\
\Theta_1(x) &= \left(E_1(x) I_1(x) \left(\frac{1}{\rho_1(x) A_1(x)} \right)'' \right)' + \varpi^2 \left(\left(\frac{E_1(x) I_1(x)}{G_1(x)} \right)' \right. \\
&\quad \left. + E_1(x) I_1(x) \left(\frac{1}{G_1(x)} \right)' + \rho_1(x) I_1(x) \left(\frac{1}{\rho_1(x) A_1(x)} \right)' \right), \\
\Theta_2(x) &= \left(2E_1(x) I_1(x) \left(\frac{1}{\rho_1(x) A_1(x)} \right)' \right)' + E_1(x) I_1(x) \left(\frac{1}{\rho_1(x) A_1(x)} \right)'' \\
&\quad + \varpi^2 \left(\frac{E_1(x) I_1(x)}{G_1(x)} + \frac{\rho_1(x) I_1(x)}{\rho_1(x) A_1(x)} \right), \\
\Theta_3(x) &= \left(\frac{E_1(x) I_1(x)}{\rho_1(x) A_1(x)} \right)' + 2E_1(x) I_1(x) \left(\frac{1}{\rho_1(x) A_1(x)} \right)', \\
\Theta_4(x) &= \frac{E_1(x) I_1(x)}{\rho_1(x) A_1(x)}.
\end{aligned} \tag{30}$$

When taking the Jacobian of Eq. (29) with respect to a_i, the only remaining unknown in the governing system determinant is the cyclic frequency ϖ^2. A successful nontrivial solution of the characteristic equation of the governing determinant gives the cyclic frequencies.

Boundary Conditions for HWM-A

The same boundary conditions as those shown in Table 1 for HWM-C are applicable to HWM-A. However, new expressions are required to define $w(x)$, $\theta(x)$, $Q(x)$, and $M(x)$ in terms of the auxiliary function $\Gamma(x,\ t)$. Therefore, the functions that define the relationships between $w(x)$, $\theta(x)$, $Q(x)$, and $M(x)$ with $\Gamma(x,\ t)$ may be provided following Huang et al.'s [7] approach,

$$w(x) = \frac{\rho_1(0) I_1(0)}{\rho_1(x) A_1(x)} \Gamma'(x), \tag{31}$$

$$\theta(x) = -\varpi^2 \frac{\rho_1(0) I_1(0)}{G_1(x)} - \left(\frac{\rho_1(0) I_1(0)}{\rho_1(x) A_1(x)} \Gamma'(x)\right)', \tag{32}$$

$$Q(x) = -\varpi^2 \frac{\rho_1(0) I_1(0)}{G_1(x)}, \tag{33}$$

$$M(x) = -E(x) I(x) \left[\varpi^2 \left(\frac{\rho_1(0) I_1(0)}{G_1(x)}\right)' + \left(\frac{\rho_1(0) I_1(0)}{\rho_1(x) A_1(x)} \Gamma'(x)\right)''\right]. \tag{34}$$

3 Results and Discussions

In this section, first, verifications are given, and then, frequency predictions for some support conditions that are not detailed in the literature, are presented.

The cross-sectional profiles utilised for the beam in the analyses are defined with, Case I: $A = A_0(1 - cx_l)$, $I = I_0(1 - cx_l)^3$ and Case II: $A = A_0(1 - cx_l)^2$, $I = I_0(1 - cx_l)^4$, where c is the taper ratio. In these cases, at the left end ($x = 0$) the cross-sectional properties are given with A_0 and I_0. c varies between 0 and 1, and where case $c = 1$ is practically meaningless. The case where $c = 0$ corresponds to a uniform cross-sectioned beam. The material properties that vary along the beam axis fit the power-law form and can be defined as follows [3]: the modulus of elasticity is $E(x_l) = E_0 + (E_1 - E_0)(x_l)^n$, and the density is $\rho(x_l) = \rho_0 + (\rho_1 - \rho_0)(x_l)^n$, where n is the gradient parameter and $n = 0$ implies the homogeneous material. Subindices 0 and 1 indicate the material properties at the left and right ends, respectively. In the present work, the materials are assumed to be zirconia and aluminum with corresponding properties of ZrO_2: $E_0 = 200\,\text{GPa}$, $\rho_0 = 5700\,\text{kg/m}^3$ and Al: $E_1 = 200\,\text{GPa}$, $\rho_1 = 5700\,\text{kg/m}^3$. In all the numerical calculations, r^2, Poisson's ratio (ν), and the shear correction factor (k) are set to 0.01, 0.3 and 5/6, respectively.

Before we start, we note that the grid point spacings are equal in all analyses. Another point that should be noted is that when a high taper ratio and material change are considered, the most challenging case appears. This case, which involves uniform cross-sections and materials, is easier because some of the derivative terms are zero because of the constant material and cross-sectional properties. Thus, we conducted several analyses with different beam support conditions and high taper ratios considering Case I for the convergence study. It is a well-known fact that support conditions strongly affect the vibration frequencies [3,7]. Hence different support conditions may require different convergence rates. First, the C-F beam results when different J values are employed to obtain the optimal resolution are compared with those of Shahba et al. [3] in Table 2.

Table 2: First four non-dimensional natural frequencies for the C-F beam (Case I, $n = 2$ and $c = 0.8$)

		HWM-C				HWM-A			
ϖ_i	[3]	$J = 2$	$J = 3$	$J = 4$	$J = 5$	$J = 2$	$J = 3$	$J = 4$	$J = 5$
1	4.718	4.1979	4.6273	4.6947	4.7103	4.7187	4.7163	4.7156	4.7154
2	13.4793	10.5789	12.9277	13.3366	13.4326	13.4722	13.4679	13.4651	13.4644
3	25.9735	19.6389	24.6163	25.6143	25.8482	26.0059	25.9610	25.9349	25.9275
4	40.8666	32.6386	38.6367	40.2363	40.6132	41.0942	40.9074	40.7837	40.7489
Deviation from [3] (%)									
		HWM-C				HWM-A			
	ϖ_i	$J = 2$	$J = 3$	$J = 4$	$J = 5$	$J = 2$	$J = 3$	$J = 4$	$J = 5$
1		11.0240	1.9228	0.4949	0.1637	0.0144	0.0363	0.0505	0.0541
2		21.5174	4.0921	1.0587	0.3466	0.0530	0.0847	0.1051	0.1109
3		24.3886	5.2252	1.3830	0.4823	0.1248	0.0482	0.1488	0.1770
4		20.1337	5.4566	1.5423	0.6200	0.5570	0.0997	0.2029	0.2881

As expected, we realise from Table 2 that higher resolution provides better results for HWM-C. However, HWM-A yields better results at resolution level 3 for all frequencies. Usually, the Haar wavelet method suggests better accuracy with higher resolution, but the use of an auxiliary function suggests an optimal resolution. Notably, higher resolution levels lead to increased computational time. To provide some data as an example of calculation speed: HWM-C calculations take approximately 2, 14 min, 2 h, and over 24 h for resolution levels ranging from 2 to 5, respectively. In comparison, HWM-A calculations take approximately 1, 8 s, 5 min, and up to 16 h for the same resolution levels. All calculations were performed on a laptop equipped with an Intel second-generation i7-7700HQ@2.80 GHz processor.

Fig. 1 illustrates the first mode shapes corresponding to the frequencies in Table 2 for both methods. Fig. 1a displays all resolution levels listed in Table 2, while Fig. 1b is shown for $J = 3$ for comparison. From the analysis of Fig. 2, it is evident that HWM-C represents a coarser approach and fails to fully capture the displacements of the first mode for the cantilever beam. This explains why HWM-C lacks sufficient sensitivity in frequency estimation especially at lower resolutions. While HWM-C calculates a mode shape similar to a uniform, homogeneous beam, HWM-A presents a sharper curve, starting at zero displacement on the left boundary and reaching maximum displacement, because a high taper ratio and material graduation causes decreasing stiffness towards the right end. The mode shape calculated with HWM-A is intuitively reasonable.

Next, to present an unusual result we provide Table 3. We consider a C-C supported beam with a homogeneous material ($n = 0$), Case I, and $c = 0.8$. As shown in Table 3, HWM-C calculates an extra frequency in the first line, which we indicate with the index 0. The fact that other frequencies closely match those reported by Huang et al. [7] suggests that the HWM-C formulation is correct but imperfect. However, this extra frequency, which decreases as the resolution increases, significantly affects the value of the first frequency. The extra frequency which does not appear in HWM-A solutions, occurs only in the C-C and C-P support conditions while using HWM-C and may stem from

the complicated boundary condition equations. We should note that this extra frequency emerges with a taper and increases in value with higher taper ratios: the additional frequency did not appear for the uniform beam. The optimal resolution is $J = 5$ for both HWM-A and HWM-C.

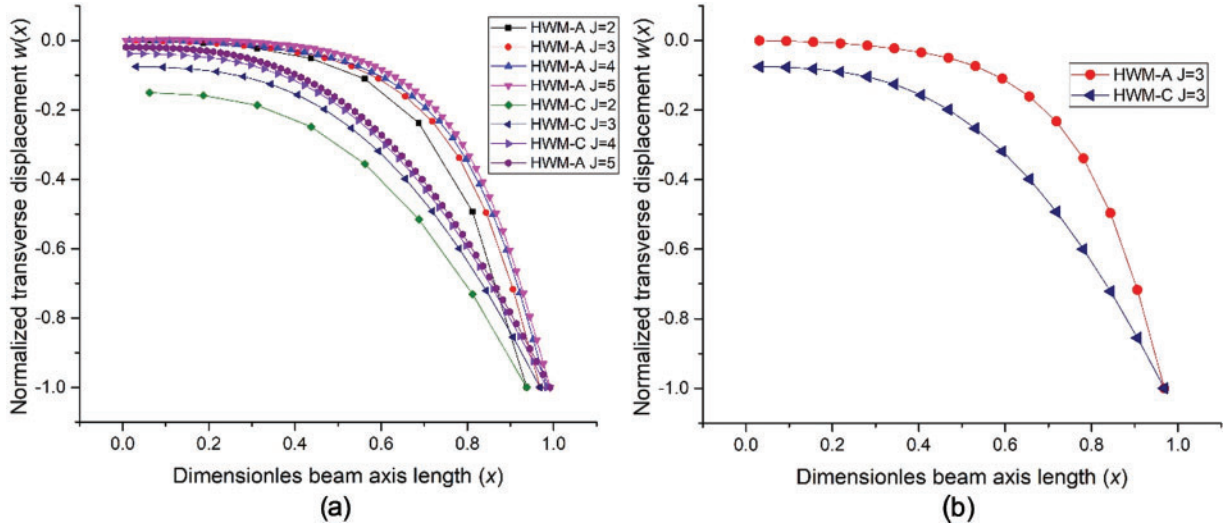

Figure 1: Transverse displacement mode shapes of C-F beam for different resolution levels: (a) A complete comparison of mode shapes for HWM-A and HWM-C, (b) A closer look at HWM-A and HWM-C at resolution level 3 (Case I, $n = 2$ and $c = 0.8$)

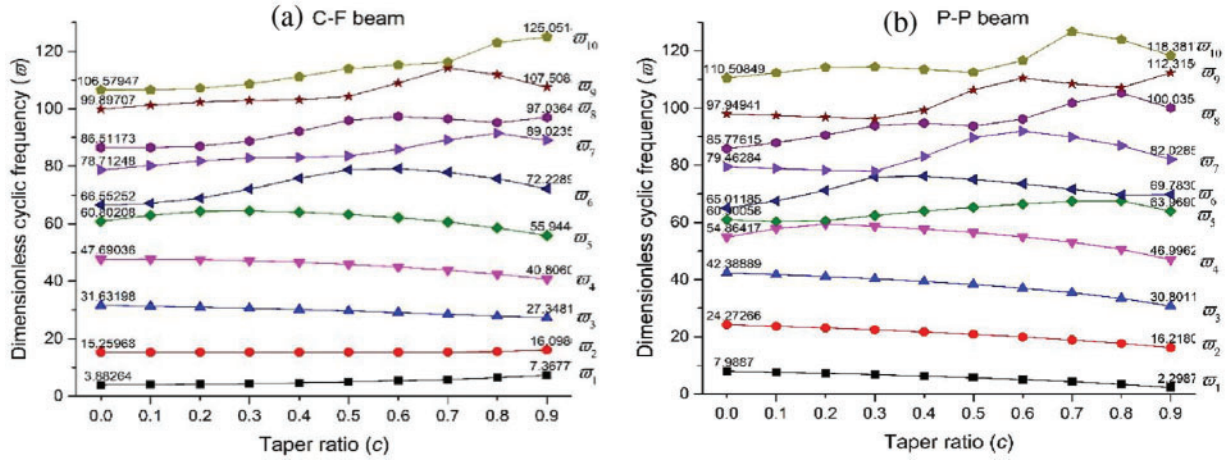

Figure 2: (Continued)

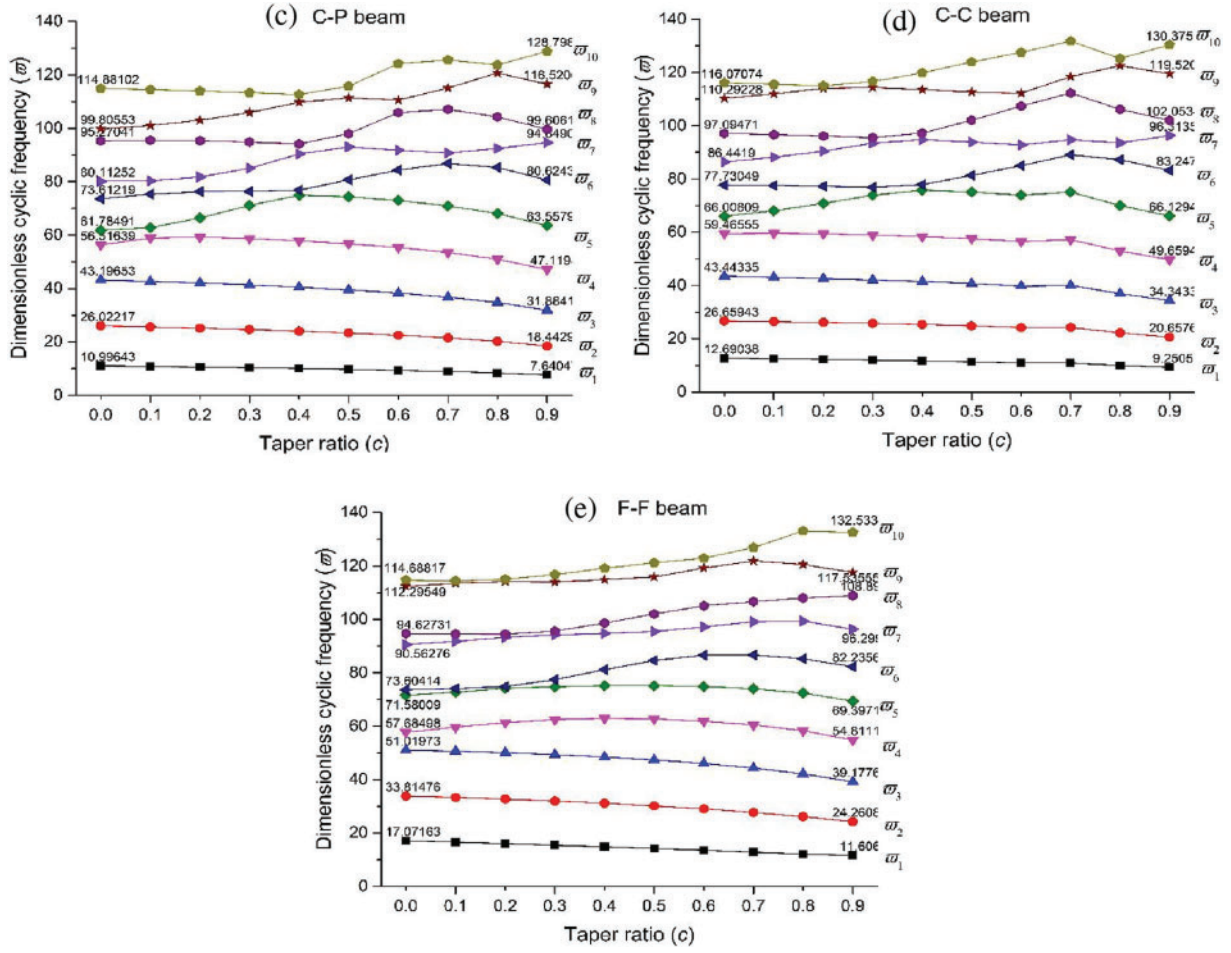

Figure 2: The variations in the dimensionless cyclic frequencies of Timoshenko beams with the taper ratio (Case II, n = 2): (a) C-F beam, (b) P-P beam, (c) C-P beam, (d) C-C beam and (e) F-F beam

As a remedy for the inaccurate results of HWM-C, the non-uniform Haar wavelets mentioned earlier can be employed. We stated that for the sake of brevity, we do not present how the non-uniform Haar wavelets are calculated. We encourage the reader to refer to Lepik et al. [37] for detailed information about non-uniform Haar wavelets. To provide a brief knowledge, the non-linear Haar wavelets utilise the denser grid spacings where needed. In our case, the critical zone is the end of the beam because high taper ratios require the calculation of more precise cross-sectional properties, especially at the right boundary. Let us introduce the parameter q, which identifies the grid spacing at the end zone of the beam using the geometric series rule. When q is close to 1, the grid spacing is uniform, and the range [0.6, 0.9] produces meaningful grid spacings. We present Table 4, which includes the HWM-C results for $J = 4$, to demonstrate the improved accuracy when $q = 0.8$ and $q = 0.9$ are used. However, while the first frequency shows good accuracy, there is still an extra frequency. Moreover, starting from the second frequency, the results begin to diverge compared with the equally spaced grid situation. This divergence accelerates from the sixth frequency for $q = 0.8$ because of the less dense grids at the beginning of the beam. Table 4 indicates that the quantities at the end boundary must be accurately calculated to estimate the frequencies successfully. Because the

Haar wavelet method transforms the boundary value problem into an initial value problem using the quantities at the end boundary. However, we should point out that this does not mean that the values at the end boundary directly affect the lowest frequencies that might be interpreted from Table 4. The values at both the left and right boundaries, as well as the grid spacing, should affect the frequencies. With a well-estimated transverse beam deflection curve, which is possible with equal grid spacing, the most accurate frequencies can be obtained. The accuracy of this judgment is demonstrated by the results of the HWM-A with equal grid spacing in Tables 2 and 3. Although the HWM-C produces accurate frequency estimations for the C-F beam at high resolutions, the results for the C-C beam are not as satisfactory as those of the HWM-A.

Table 3: First five non-dimensional natural frequencies for the C-C beam (Case I, $n = 0$ and $c = 0.8$)

		HWM-C				HWM-A			
ϖ_i	[7]	$J = 2$	$J = 3$	$J = 4$	$J = 5$	$J = 2$	$J = 3$	$J = 4$	$J = 5$
0	–	5.5126	4.5171	2.79190	1.4787	–	–	–	–
1	9.7271	16.4847	12.6633	10.45904	9.9052	9.7287	9.7244	9.7263	9.7269
2	22.4303	32.5146	23.9143	22.69676	22.4919	22.6479	22.4824	22.4431	22.4336
3	37.7417	59.1315	37.8607	37.72293	37.7353	38.5710	37.9764	37.8019	37.7572
4	54.4994	88.2081	53.7582	54.31274	54.4493	56.5165	55.1534	54.6670	54.5384
5	71.9943	93.2928	71.1183	71.85737	72.0220	75.6616	73.5203	72.4624	72.1738
		Deviation from [7] (%)							
		HWM-C				HWM-A			
ϖ_i		$J = 2$	$J = 3$	$J = 4$	$J = 5$	$J = 2$	$J = 3$	$J = 4$	$J = 5$
0		–	–	–	–	–	–	–	–
1		69.4715	30.1849	7.5242	1.8301	0.0158	0.0278	0.0091	0.0021
2		44.9585	6.6161	1.1880	0.2745	0.9702	0.2325	0.0572	0.0149
3		56.6743	0.3152	0.0497	0.0171	2.1974	0.6218	0.1594	0.0411
4		61.8517	1.3600	0.3424	0.0918	3.7012	1.2001	0.3076	0.0716
5		29.5836	1.2167	0.1901	0.0385	5.0939	2.1197	0.6502	0.2493

Table 4: First ten non-dimensional natural frequencies for the C-C beam ($J = 4$, Case I, $n = 0$ and $c = 0.8$)

		HWM-C		
ϖ_i	[7]	$q = 0.8$	$q = 0.9$	Uniform grid spacing
0	–	1.7717	1.1023	2.7919
1	9.7271	9.7457	9.7457	10.4590
2	22.4303	21.4216	21.4216	22.6968
3	37.7417	36.0785	36.0785	37.7229

(Continued)

Table 4 (continued)

		HWM-C		
ϖ_i	[7]	$q = 0.8$	$q = 0.9$	Uniform grid spacing
4	54.4994	53.1228	53.1228	54.3127
5	71.9943	72.4012	72.4012	71.8574
6	–	92.0828	89.8013	89.0195
7	–	95.1446	93.7853	93.7418
8	–	122.8103	110.4052	108.9680
9	–	124.4464	123.7054	123.4165
10		153.7935	129.8417	128.3750

Although the success of HWM-C was demonstrated by Hein et al. [38] for the Euler–Bernoulli beam, which has relatively simple governing equations, our results show that a new approach is required for the Timoshenko beam, whose governing equations are more complex. Many attempts have been made to solve this problem while considering different support conditions, which are not presented here for the sake of brevity, and HWM-C did not yield satisfactory results for all the cases. Since the results of HWM-C are not satisfactory, we present the results obtained using HWM-A.

Tables 2 and 3 offer the different optimal resolutions needed for the C-F and C-C support conditions when HWM-A is employed. To determine the optimum resolution level for the remaining C-P, P-P, and F-F beams, we perform HWM-A analyses with different resolution levels. We compare them with solutions available in the literature in Tables 5–7, respectively. Table 5 indicates that the optimal resolution is 5 for the C-P beam, and the deviations are acceptably small for all values of J.

Table 5: First four non-dimensional natural frequencies for the C-P beam (Case I, $n = 2$ and $c = 0.1$)

		HWM-A				Deviation from [7] (%)			
ϖ_i	[7]	$J = 2$	$J = 3$	$J = 4$	$J = 5$	$J = 2$	$J = 3$	$J = 4$	$J = 5$
1	10.8007	10.8310	10.8085	10.8027	10.8012	0.2807	0.0721	0.0181	0.0045
2	25.6179	25.9015	25.6933	25.6370	25.6227	1.1072	0.2943	0.0746	0.0187
3	42.6478	43.7597	42.9578	42.7268	42.6674	2.6071	0.7270	0.1852	0.0459
4	58.8595	59.6760	59.2491	58.9673	58.8824	1.3873	0.6619	0.1833	0.0390

Table 6: First four non-dimensional natural frequencies for the P-P beam (Case I, $n = 2$ and $c = 0.9$)

		HWM-A				Deviation [3] (%)			
ϖ_i	[3]	$J = 2$	$J = 3$	$J = 4$	$J = 5$	$J = 2$	$J = 3$	$J = 4$	$J = 5$
1	3.2016	3.3060	3.2143	3.1918	3.1864	3.2609	0.3965	0.3049	0.4741
2	15.3775	15.8036	15.4374	15.3496	15.3284	2.7712	0.3898	0.1817	0.3191

(Continued)

Table 6 (continued)

		HWM-A				Deviation [3] (%)			
ϖ_i	[3]	$J=2$	$J=3$	$J=4$	$J=5$	$J=2$	$J=3$	$J=4$	$J=5$
3	29.9011	31.2568	30.1279	29.8572	29.7912	4.5339	0.7586	0.1468	0.3675
4	46.2153	49.3104	46.7740	46.1476	45.9919	6.6972	1.2090	0.1465	0.4833

Table 7: First five non-dimensional natural frequencies for the F-F beam (Case I, $n=0$ and $c=0.2$)

		HWM-A				Deviation from [20] (%)			
ϖ_i	[20]	$J=2$	$J=3$	$J=4$	$J=5$	$J=2$	$J=3$	$J=4$	$J=5$
1	15.7200	15.6725	15.7118	15.7211	15.7234	0.3023	0.0524	0.0071	0.0218
2	32.7900	32.8776	32.8185	32.7941	32.7874	0.2670	0.0869	0.0124	0.0080
3	50.6800	51.2065	50.9027	50.7660	50.7282	1.0388	0.4394	0.1696	0.0951
4	61.0500	63.6619	62.6475	62.3328	62.2508	4.2784	2.6167	2.1012	1.9669
5	66.9400	76.6140	76.4790	76.0044	75.8539	14.4517	14.2501	13.5411	13.3163

Table 6 compares the P-P beam results with those of Shahba et al. [3], considering Case I, for the highest taper ratio. From Table 6 the optimal resolution may be determined to be 4.

Table 7 compares the results given by Leung et al. [20] for a homogeneous F-F beam with a taper ratio of 0.2. Table 7 suggests that the optimal resolution for the F-F beam is 5.

From Table 7, it is apparent that there are relatively high deviations from Leung et al. [20] for the fourth and fifth frequencies. Shahba et al. [3] and Huang et al. [7] reported similar deviations from Leung et al. [20] for the fourth and fifth frequencies when the taper ratios were considered. This may be due to the method of Leung et al. [20], as Shahba et al. [3] and Huang et al. [7] are consistent with each other.

To the best of the authors' knowledge, solutions for Timoshenko beams with axial FG materials and variable cross-sections using HWM-C have been provided in the literature only for the C-C beam by Lepik et al. [37]. Unfortunately, Lepik et al. [37] did not specify the value of J in their study. In Table 8, we compare the limited data provided by Lepik et al. [37] with our HWM-A for Cases I and II cross-section variations. In our HWM-A analyses, we employed J as 4 which is a relatively low resolution. The computational time is a maximum of 15 min. Table 8 shows that the HWM-A results are closer to those of Shahba et al. [3]. The results presented thus far suggest that HWM-A provides more stable and accurate results than HWM-C does, even at low resolutions.

Table 8: First five non-dimensional natural frequencies for the C-C beam (Cases I and II, $n = 2$)

		$c = 0.1$			$c = 0.5$			$c = 0.7$		
	ϖ_i	[3]	[37]	HWM-A	[3]	[37]	HWM-A	[3]	[37]	HWM-A
Case I	1	12.4689	12.4577	12.4664	11.1706	11.1699	11.1663	10.1036	10.1212	10.0938
	2	26.4153	26.3780	26.3982	24.6797	24.6430	24.6642	22.9773	22.9460	22.9559
	3	43.0904	–	43.0326	40.6374	–	40.5859	38.3161	–	38.2642
	4	59.6829	–	59.5916	57.5925	–	57.4754	54.9627	–	54.8499
Case II	1	12.4812	12.4697	12.4783	11.3199	11.3140	11.3123	10.4579	10.5004	10.4434
	2	26.4376	26.3922	26.4198	24.8744	24.8243	24.8511	23.3976	23.4245	23.3911
	3	43.1098	–	43.0506	40.7919	–	40.7262	38.6570	–	38.7132
	4	59.7067	–	59.6133	57.7257	–	57.5864	55.2354	–	55.4816

Our final comparison is with experimental data provided by Díaz-De-Anda et al. [34] for the first ten frequencies in Table 9. Díaz-De-Anda et al. [34] conducted experiments on an F-F beam with a homogeneous, uniform cross-section and a length of 0.5 m. The rectangular beam has dimensions of 0.0252 m in height and 0.0504 m in width. The beam material is aluminum with elastic constants of $G = 26.92$ GPa, $E = 67.42$ GPa, and $\rho = 2699.04$ kg/m^3. Table 9 shows HWM-A estimates frequencies with less than 6% deviation.

Table 9: First ten experimental and numerical natural frequencies of the uniform and homogenous F-F beam

Frequency no.	[34] (kHz)	HWM-A (kHz)	Deviation from [34] (%)
1	1.0211	1.0001	2.0566
2	2.6594	2.6480	0.4287
3	4.8462	4.9083	1.2812
4	7.3878	7.5859	2.6817
5	10.1630	10.5299	3.6101
6	13.0820	13.6320	4.2042
7	16.0810	16.8227	4.6120
8	19.1335	20.0599	4.8420
9	22.1699	23.3197	5.1862
10	25.1638	26.5882	5.6607

Table 10 lists the first 15 frequencies for the C-P and F-F beams, for which detailed results have not been presented in the literature. In the table, the material non-homogeneity parameter is $n = 2$. Table 10 shows that the difference between the C-P beam and the F-F beam frequencies is very noticeable up

to the fourth frequency. However, the frequencies of the C-P and F-F beams are closer, starting from the fourth frequency to the 15th. With increasing taper ratios, the higher frequencies of the C-P and F-F beams become closer to each other. This trend can be interpreted as the high-order frequencies are being influenced by the mass—stiffness distribution along the beam axis rather than the support condition's effect. The effect of support conditions is more noticeable at lower frequencies.

Table 10: First fifteen dimensionless natural frequencies of the axially FG material C-P and F-F beam for various taper ratios (Case I, $n = 2$)

	ϖ_i	$c = 0$	$c = 0.1$	$c = 0.2$	$c = 0.3$	$c = 0.4$	$c = 0.5$	$c = 0.6$	$c = 0.7$	$c = 0.8$	$c = 0.9$
	1	10.9964	10.8012	10.5822	10.3353	10.0551	9.7338	9.3604	8.9170	8.3705	7.6405
	2	26.0222	25.6227	25.1677	24.6469	24.0460	23.3447	22.5125	21.5000	20.2160	18.4430
	3	43.1965	42.6674	42.0558	41.3438	40.5062	39.5066	38.2901	36.7662	34.7662	31.8842
	4	56.3164	58.8824	59.2303	58.6985	57.8549	56.7513	55.3358	53.4855	50.9522	47.1198
	5	61.7849	62.8002	66.4477	71.1663	74.9179	74.3477	72.9432	70.9583	68.1016	63.5580
	6	73.6122	75.2986	76.2944	76.3285	76.7996	80.6812	84.3268	86.7889	85.3831	80.6244
	7	80.1125	80.3514	81.7727	85.0543	90.3751	92.9988	91.7425	90.7574	92.4073	94.6491
C-P	8	95.2704	95.5331	95.3532	94.8568	94.1279	97.9649	105.8898	107.1004	104.2675	99.6061
	9	99.8055	101.0384	103.0539	105.8854	109.7266	111.3480	110.5784	115.0975	120.7066	116.5206
	10	114.8810	114.4861	113.9819	113.3520	112.6368	115.7808	124.2037	125.5652	123.7654	128.7987
	11	124.0349	125.6341	127.5851	129.8237	130.4467	129.6172	129.0225	137.8627	140.5140	135.0837
	12	133.2043	132.7968	132.3334	131.9911	133.8761	138.2347	143.9649	143.8232	149.1923	152.6739
	13	150.1412	150.3110	150.0138	149.4862	148.7727	147.8929	147.9408	158.7598	158.9928	159.7353
	14	152.0448	152.9196	154.4953	156.6254	159.3984	162.7985	163.7761	162.0875	174.2421	171.1580
	15	169.0249	168.6553	168.2072	167.6615	167.0175	166.5841	170.1403	180.2620	177.6932	188.1509
	1	17.0716	16.5503	16.0003	15.4200	14.8070	14.1654	13.4963	12.8102	12.1401	11.6060
	2	33.8148	33.3016	32.6883	31.9684	31.1371	30.1654	29.0339	27.7056	26.1286	24.2608
	3	51.0197	50.6121	50.0435	49.3213	48.4682	47.3778	46.0318	44.3416	42.1534	39.1777
	4	57.6850	59.6283	61.3218	62.4246	62.9118	62.6676	61.8512	60.4394	58.2555	54.8111
	5	71.5801	72.7312	74.1678	74.7179	75.1535	75.1775	74.8459	74.0165	72.4207	69.3972
	6	73.6041	74.0248	74.8526	77.4651	81.1189	84.5759	86.5536	86.6268	85.2351	82.2356
	7	90.5628	91.7523	93.2736	94.1475	94.7219	95.4412	97.1416	99.0931	99.2964	96.2995
F-F	8	94.6273	94.5008	94.4362	95.6054	98.6030	102.0282	105.0827	106.6605	107.9827	108.8937
	9	112.2955	113.5096	114.1515	113.9776	114.8797	115.8903	119.1848	121.8414	120.5304	117.5356
	10	114.6882	114.4199	114.9922	116.7473	119.1045	121.1738	122.8854	126.9020	133.0631	132.5338
	11	133.7703	133.6223	133.4890	133.4811	135.2645	136.5553	140.1632	142.0040	140.9890	143.3065
	12	136.6780	137.6167	138.7024	139.8665	141.4077	142.3655	142.7611	148.0316	155.3155	152.8391
	13	152.7509	152.7397	152.8485	153.2213	156.1754	157.8638	160.8963	162.0244	163.6787	168.7078
	14	161.8345	162.2689	162.6432	162.8865	163.9899	164.1129	164.3775	169.2516	175.1003	175.4095
	15	172.5452	172.9410	173.6007	174.6636	178.4645	180.4309	182.5774	183.1778	188.0462	189.5659

Fig. 2 shows the variation in the natural frequencies of Timoshenko beams with respect to the taper ratio considering Case II for five different support conditions. From Fig. 2, a general evaluation may be given: for all beams, the first four frequencies decrease with increasing taper ratio except for the C-F beam. While the first two frequencies increase with increasing taper ratio for the C-F beam, the third and fourth frequencies exhibit a similar trend with the general evaluation. The same conclusion was reported by Shahba et al. [3]. Moreover, an increase in the fourth frequency of the P-P beam for $c = 0.2$ is also observed, as reported by Shahba et al. [3]. The variations in the first four frequencies with respect to the taper ratio are nearly linear for all support cases of the Timoshenko beams. Starting from the fifth frequency, the higher-order frequencies do not exhibit a systematic trend: highly oscillating frequencies have been observed at particularly higher taper ratios for higher-order frequencies. The F-F beam has the most ordered frequency variation with the taper ratio.

The effect of the taper ratio on the mode shapes is another focus of this study. To illustrate this effect, Fig. 3 presents the variation of the first mode shapes *vs*. the taper ratio. Fig. 3 summarizes the analyses of Case I with a material gradation coefficient of $n = 2$. To avoid clutter, mode shapes corresponding to critical taper ratio changes are displayed for selected beam support cases, while in some cases, more mode shapes are provided to describe the trend clearly. A general observation from Fig. 3 is that, except for the F-F beam case, the curvature centre of the axis of the beam changes direction after $c = 0.5$ in other support conditions, while in the F-F case, this change begins at $c = 0.3$. A significant change is observed in the mode shapes of all beam types as the taper ratio increases. The stiffness, which decreases towards the right end of the beam due to the taper ratio and material gradation, shifts the largest displacement towards the beam's right end. Two noteworthy cases are highlighted in Fig. 3a–e: (i) Beam behaviour with decreasing stiffness towards the right end resembles the mode shape of a cantilever beam. (ii) As shown in Fig. 3e, the decreasing stiffness creates an ideal cantilever mode shape in the F-F beam with high taper ratio, almost as if pseudo support were present at the left end.

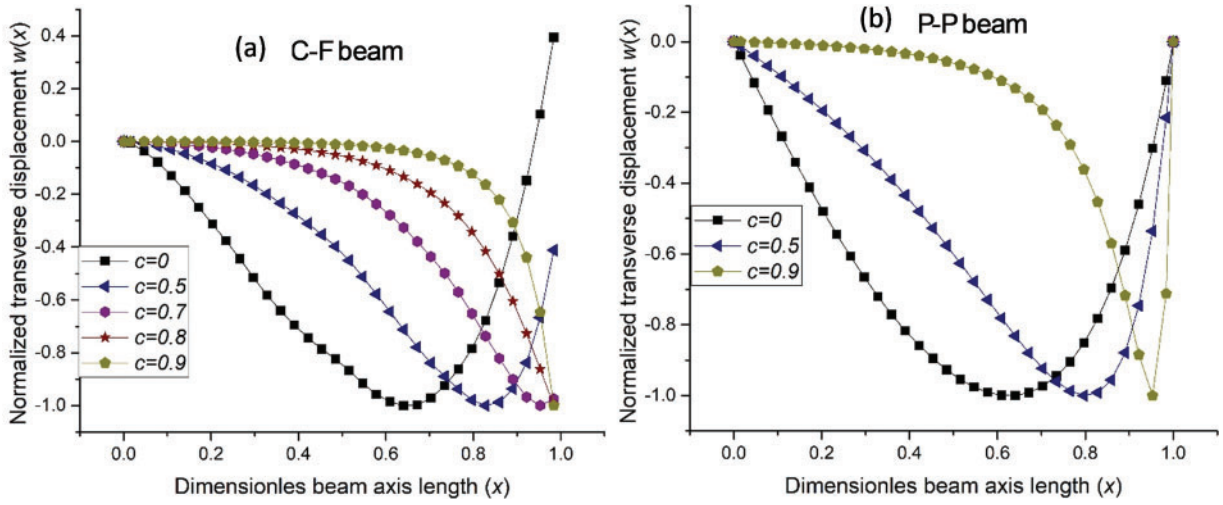

Figure 3: (Continued)

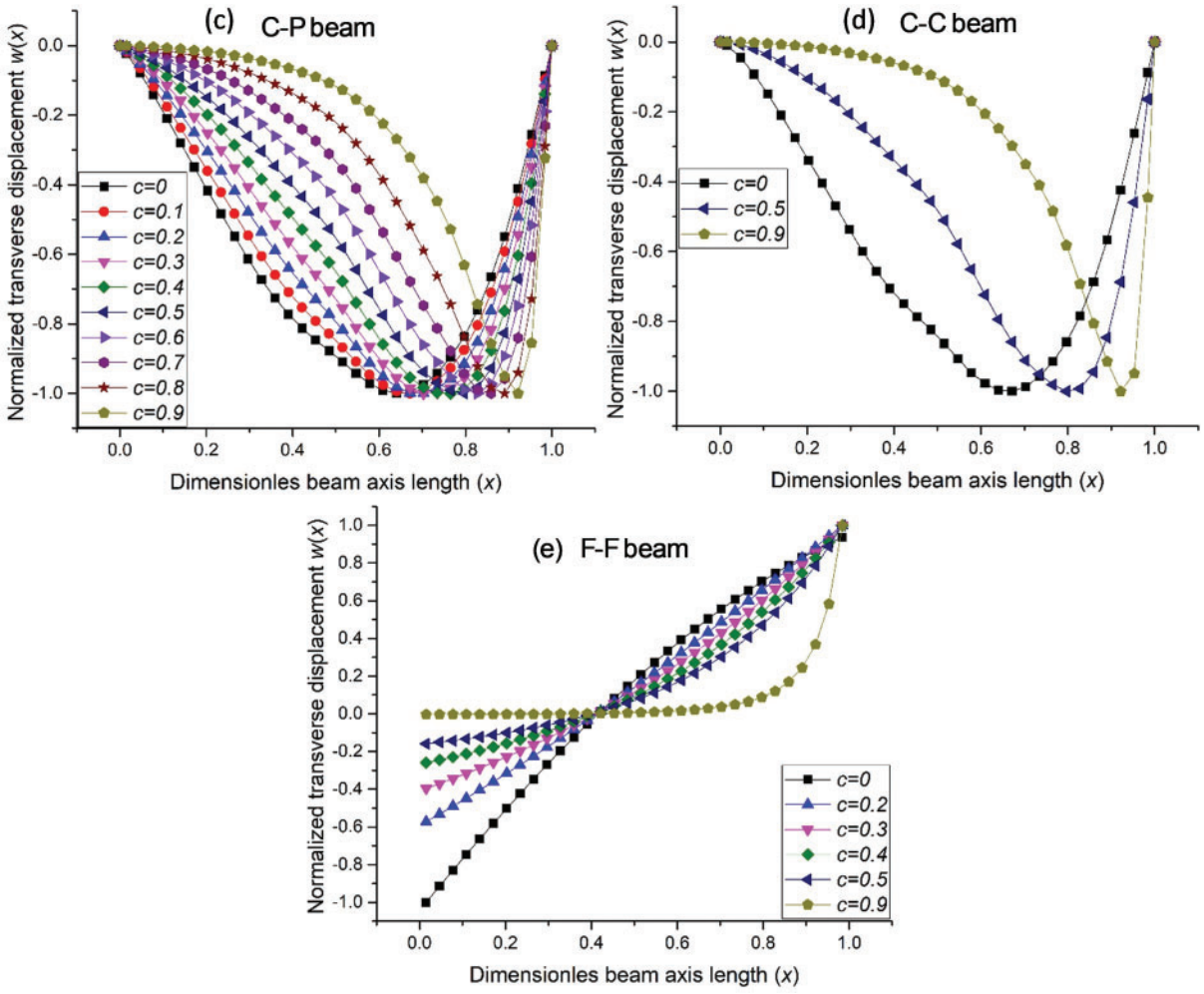

Figure 3: Variation of the first mode shapes of Timoshenko beams for the different taper ratios (Case I, n = 2): (a) C-F beam, (b) P-P beam, (c) C-P beam, (d) C-C beam and (e) F-F beam

For an interpretation of the relation between natural frequencies and beam taper, Fig. 4 is provided. Fig. 4 illustrates the variation of the first 24 frequencies of an F-F beam along the taper ratio for Case I (homogeneous wedge beam) and Case II (homogeneous cone beam). As reported by Shahba et al. [3] and Huang et al. [7], the impact of material gradation on frequencies is minimal; therefore, a homogeneous material beam was analysed. In Fig. 4, the horizontal bars and the numbers next to the bars represent the frequencies and the frequency indices from lowest to highest order, respectively. The beam material is aluminum, with material properties and other analysis parameters as specified at the beginning of Section 3. The uniform case is represented by $c = 0$ in Fig. 4 as a benchmark case. It should be noted that in some taper ratio scenarios, frequencies above 300 have been excluded from the figure.

In both cases shown in Fig. 4, it is noteworthy that beyond a certain frequency, the frequencies appear in closely spaced pairs. This phenomenon is especially evident just after the first four modes in the uniform and low taper ratios. As the taper ratio increases beyond $c = 0.3$, the frequency overlaps shift to higher-order modes and disappear entirely at $c = 0.9$. The paired frequencies can be interpreted as modes where the critical frequency is reached, and shear deformations become significant. In contrast, frequencies that are far apart and do not overlap can be associated with flexural deformations (For further readings on critical frequency and paired frequencies, please refer to references [32–36]). It is worth interpreting that at the ratio $c = 0.9$, why there is no frequency overlap within the first 24 frequencies. Examining the trend across other taper ratios, it is likely that this overlap may appear in higher-order modes beyond the 24th one. The taper ratio increases, the beam becomes more slender, and the beam behaviour becomes increasingly dominated by flexural deformations. That's why the overlapping frequencies shift towards the higher-order modes.

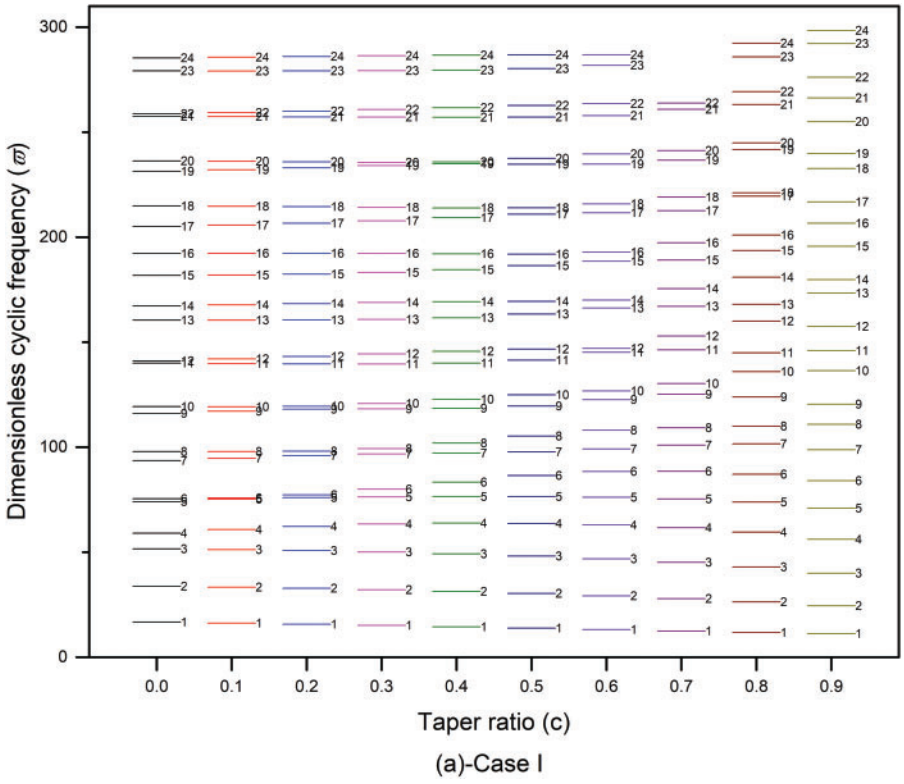

Figure 4: (Continued)

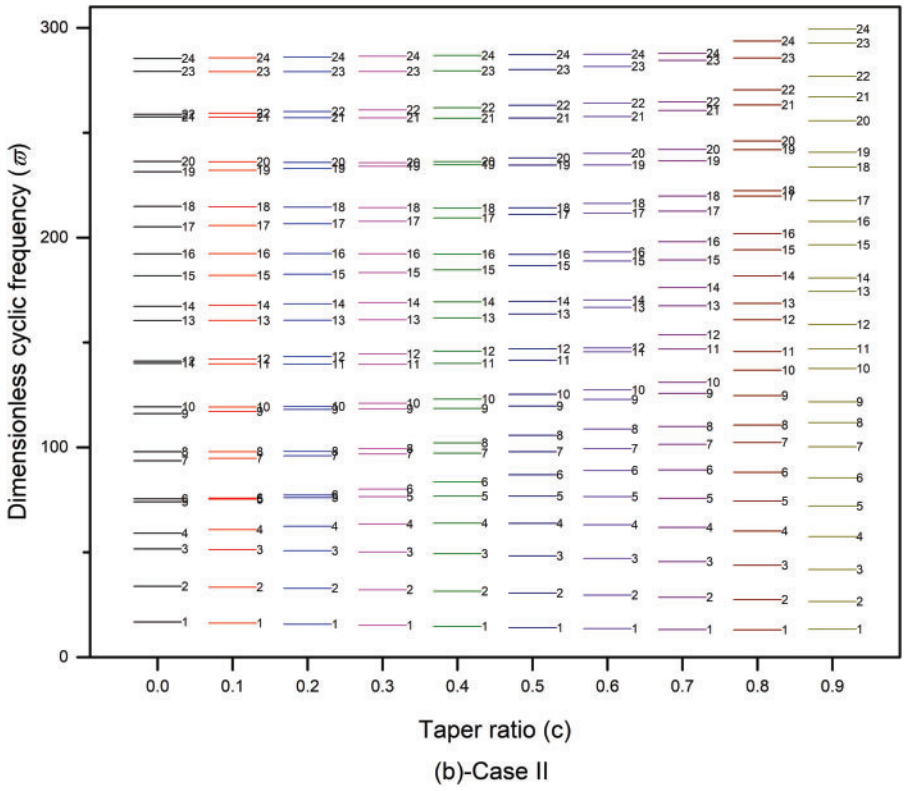

Figure 4: Variation of the first 24 dimensionless frequencies of homogeneous F-F beam *vs*. taper ratio: (a) Case I (tapered beam), (b) Case II (cone beam)

4 Conclusions

In this work, the free vibration of variable cross-section Timoshenko beams with FG material was investigated using Haar wavelets. The method was applied using two different approaches called HWM-C and HWM-A. In both approaches, coupled governing differential equations are reduced to a single differential equation. The equation coefficients are then arranged for the solution function. With discretization, the equations that become a system of linear equations are solved, and the frequencies are determined. The most important difference between the methods is that in the HWM-C, the resultant function is directly equal to the beam cross-section rotation, whereas in the HWM-A, rotation, and deflection are derived from an auxiliary function. It has been shown through many comparisons that while HWM-C yields results compatible with the literature only under certain support conditions, HWM-A yields results that are more compatible with the literature under all conditions at lower resolutions. The Haar wavelet method can be increased with the alternative function approach. The frequency estimations of some support conditions for which detailed results are not given in the literature are presented.

Considering a certain material change situation, the variation of the free vibration frequencies with respect to taper ratios of Timoshenko beams with different supports are presented with graphs for the first 10 frequencies. In addition, the variations of the first mode shapes with respect to the taper ratio for all support types are presented to provide further insight into the behaviour of auxiliary FG beams. Finally, the frequencies of a homogeneous F-F beam varying with taper ratio are also provided

as a diagram. This diagram shows the relationship between the geometric beam parameters and the natural vibration frequencies and can be used to distinguish flexural and shear modes.

Acknowledgement: Not applicable.

Funding Statement: This research did not receive any specific grant from funding agencies in the public, commercial, or not-for-profit sectors.

Availability of Data and Materials: Not applicable.

Ethics Approval: Not applicable.

Conflicts of Interest: The author declares no conflicts of interest to report regarding the present study.

References

1. Géradin M, Rixen DJ. Mechanical vibrations: theory and application to structural dynamics. 3rd ed. West Sussex: John Wiley and Sons; 2015.
2. Elishakoff I. Who developed the so-called Timoshenko beam theory? Math Mech Solids. 2020;25:97–116. doi:10.1177/1081286519856931.
3. Shahba A, Attarnejad R, Marvi MT, Hajilar S. Free vibration and stability analysis of axially functionally graded tapered Timoshenko beams with classical and non-classical boundary conditions. Compos B Eng. 2011;42:801–8. doi:10.1016/j.compositesb.2011.01.017.
4. Rahgozar R, Safari H, Kaviani P. Free vibration of tall buildings using Timoshenko beams with variable cross-section. WIT Trans Built Environ: Struct Mat. 2004;73:233–42.
5. Li H, Balachandran B. Buckling and free oscillations of composite microresonators. J Microelectromech Sys. 2006;15:42–51. doi:10.1109/JMEMS.2005.863598.
6. Sears A, Batra RC. Macroscopic properties of carbon nanotubes from molecular-mechanics simulations. Phys Rev B Condens Matter Mater Phys. 2004;69(23):235406. doi:10.1103/PhysRevB.69.235406.
7. Huang Y, Yang LE, Luo QZ. Free vibration of axially functionally graded Timoshenko beams with non-uniform cross-section. Compos B Eng. 2013;45(1):1493–8. doi:10.1016/j.compositesb.2012.09.015.
8. Li XF. A unified approach for analyzing static and dynamic behaviors of functionally graded Timoshenko and Euler-Bernoulli beams. J Sound Vib. 2008;318(4–5):1210–29. doi:10.1016/j.jsv.2008.04.056.
9. Benatta MA, Tounsi A, Mechab I, Bachir Bouiadjra M. Mathematical solution for bending of short hybrid composite beams with variable fibers spacing. Appl Math Comput. 2009;212(2):337–48. doi:10.1016/j.amc.2009.02.030.
10. Kang YA, Li XF. Large deflections of a non-linear cantilever functionally graded beam. J Reinf Plast Compos. 2010;29(2):1761–74. doi:10.1177/0731684409103340.
11. Huang TC. The effect of rotatory inertia and of shear deformation on the frequency and normal mode equations of uniform beams with simple end conditions. J App Mech. 1960;28(4):579–84. doi:10.1115/1.3641787.
12. Thomas DL, Wilson JM, Wilson RR. Timoshenko beam finite elements. J Sound Vib. 1973;31(3):315–30. doi:10.1016/S0022-460X(73)80276-7.
13. Heppler GR, Hansen JS. Timoshenko beam finite elements using trigonometric basis functions. AIAA J. 1988;26(11):1378–86. doi:10.2514/3.10051.
14. Ju F, Lee HP, Lee KH. On the free vibration of stepped beams. Int J Solids Struct. 1994;31(22):3125–37. doi:10.1016/0020-7683(94)90045-0.

15. Rossi RE, Laura PAA, Gutierrez RH. A note on transverse vibrations of a Timoshenko beam of non-uniform thickness clamped at one end and carrying a concentrated mass at the other. J Sound Vib. 1990;143(3):491–502. doi:10.1016/0022-460X(90)90738-L.
16. Loula AFD, Hughes TJR, Franca LP. Petrov-Galerkin formulations of the Timoshenko beam problem. Comput Methods Appl Mech Eng. 1987;63(2):115–32. doi:10.1016/0045-7825(87)90167-8.
17. Grosh K, Pinsky PM. Design of Galerkin generalized least squares methods for Timoshenko beams. Comput Methods Appl Mech Eng. 1996;132(1–2):1–16. doi:10.1016/0045-7825(96)01002-X.
18. Lee SY, Lin SM. Exact vibration solutions for nonuniform Timoshenko beams with attachments. AIAA J. 1992;30(12):2930–4. doi:10.2514/3.48979.
19. Tong X, Tabarrok B, Yeh KY. Vibration analysis of Timoshenko beams with non-homogeneity and varying cross-section. J Sound Vib. 1995;186(5):821–35. doi:10.1006/jsvi.1995.0490.
20. Leung AYT, Zhou WE, Lim CW, Yuen RKK, Lee U. Dynamic stiffness for piecewise non-uniform Timoshenko column by power series–part I: conservative axial force. Int J Numer Methods Eng. 2001;51(5):505–29. doi:10.1002/nme.159.
21. Reddy JN. Theory and analysis of elastic plates and shells. 2nd ed. Boca Raton: CRC Press; 2006. doi:10.1201/9780849384165-6.
22. Yuan J, Pao YH, Chen W. Exact solutions for free vibrations of axially inhomogeneous Timoshenko beams with variable cross section. Acta Mech. 2016;227:2625–43. doi:10.1007/s00707-016-1658-6.
23. Wang YQ, Zhao HL. Free vibration analysis of metal foam core sandwich beams on elastic foundation using Chebyshev collocation method. Arch App Mech. 2019;89:2335–49. doi:10.1007/s00419-019-01579-0.
24. Chen WR. Vibration analysis of axially functionally graded Timoshenko beams with non-uniform cross-section. Latin Am J Solids Struct. 2021;18(7):e397. doi:10.1590/1679-78256434.
25. Zhang P, Schiavone P, Qing H. Stress-driven local/nonlocal mixture model for buckling and free vibration of FG sandwich Timoshenko beams resting on a nonlocal elastic foundation. Compos Struct. 2022;289:115473. doi:10.1016/j.compstruct.2022.115473.
26. Zhang P, Schiavone P, Qing H. A unified local-nonlocal integral formulation for dynamic stability of FG porous viscoelastic Timoshenko beams resting on nonlocal Winkler-Pasternak foundation. Compos Struct. 2023;322:117416. doi:10.1016/j.compstruct.2023.117416.
27. Sinha A. Free vibration of a timoshenko beam with arbitrary nonuniformities, discontinuities and constraints. J Vib Eng Tech. 2023;11(5):2099–108. doi:10.1007/s42417-022-00690-x.
28. Burlayenko VN, Kouhia R, Dimitrova SD. One-dimensional vs. three-dimensional models in free vibration analysis of axially functionally graded beams with non-uniform cross-sections. Mech Compos Mat. 2024;60(1):83–102. doi:10.1007/s11029-024-10176-4.
29. Burlayenko VN, Kouhia R, Dimitrova SD. Free vibration analysis of curvilinearly tapered axially functionally graded material beams. App Sci. 2024;14(15):6446. doi:10.3390/app14156446.
30. Burlayenko VN, Altenbach H, Dimitrova SD. Modal characteristics of functionally graded porous Timoshenko beams with variable cross-sections. Compos Struct. 2024;342:118273. doi:10.1016/j.compstruct.2024.118273.
31. Deneme IO, Calim FF. An efficient numerical method for free and forced vibrations of timoshenko beams with variable cross-section. Iran J Sci Tech–Trans Civ Eng. 2024;7:1–13. doi:10.1007/s40996-024-01503-9.
32. Kaneko T. An experimental study of the Timoshenko's shear coefficient for flexurally vibrating beams. J Phys D Appl Phys. 1978;11(14):1979–88. doi:10.1088/0022-3727/11/14/010.
33. Méndez-Sánchez RA, Morales A, Flores J. Experimental check on the accuracy of Timoshenko's beam theory. J Sound Vib. 2005;279(1–2):508–12. doi:10.1016/j.jsv.2004.01.050.
34. Díaz-De-Anda A, Flores J, Gutiérrez L, Méndez-Sánchez RA, Monsivais G, Morales A. Experimental study of the Timoshenko beam theory predictions. J Sound Vib. 2012;331(26):5732–44. doi:10.1016/j.jsv.2012.07.041.

35. Monsivais G, Díaz-De-Anda A, Flores J, Gutiérrez L, Morales A. Experimental study of the Timoshenko beam theory predictions: further results. J Sound Vib. 2016;375:187–99. doi:10.1016/j.jsv.2016.04.003.
36. Brøns M, Thomsen JJ. Experimental testing of Timoshenko predictions of supercritical natural frequencies and mode shapes for free-free beams. J Sound Vib. 2019;459:114856. doi:10.1016/j.jsv.2019.114856.
37. Lepik Ü, Hein H. Haar wavelets with applications. London: Springer Science & Business Media; 2014. doi:10.1007/978-3-319-04295-4_11.
38. Hein H, Feklistova L. Free vibrations of non-uniform and axially functionally graded beams using Haar wavelets. Eng Struct. 2011;33(12):3696–701. doi:10.1016/j.engstruct.2011.08.006.
39. Mehrparvar M, Majak J, Karjust K, Arda M. Free vibration analysis of tapered Timoshenko beam with higher order Haar wavelet method. Proc Est Acad Sci. 2022;71(1):77–83. doi:10.3176/proc.2022.1.07.
40. Chen CF, Hsiao CH. Haar wavelet method for solving lumped and distributed-parameter systems. IEE Proc: Cont Theo App. 1997;144(1):87–94. doi:10.1049/ip-cta:19970702.